Recent Convection Decline in the Greenland Sea: Insights From the Mercator Ocean System Over 2008–2020

Louise Abot, Christine Provost, Léa Poli

JGR Oceans

RESEARCH ARTICLE
10.1029/2022JC019320

Recent Convection Decline in the Greenland Sea: Insights From the Mercator Ocean System Over 2008–2020

Louise Abot[1], Christine Provost[1], and Léa Poli[1]

[1]Laboratoire LOCEAN-IPSL, Sorbonne Université (UPMC, University Paris 6), CNRS, IRD, MNHN, Paris, France

Key Points:

- Mercator Ocean System well reproduced hydrographic properties and mixed layer depth evolution over the Greenland Sea from 2008 to 2020
- Maximum mixed layer depths in the Greenland Sea display a strong decline from 2015 onward in the model and in the observations
- Model convection decrease is associated with stratification changes, Atlantic Water spreading and Greenland Sea Gyre weakening

Supporting Information:

Supporting Information may be found in the online version of this article.

Correspondence to:

L. Abot,
louise.abot@locean.ipsl.fr

Citation:

Abot, L., Provost, C., & Poli, L. (2023). Recent convection decline in the Greenland Sea: Insights from the Mercator ocean system over 2008–2020. *Journal of Geophysical Research: Oceans*, *128*, e2022JC019320. https://doi.org/10.1029/2022JC019320

Received 21 SEP 2022
Accepted 15 MAY 2023

Abstract We investigated wintertime convection evolution in recent years over the Greenland Sea. This area is a major location regarding dense water production and supply of the lower limb of the Atlantic Meridional Overturning Circulation, a key component of the global climate. Previous studies mentioned an increase in Greenland Sea wintertime convection intensity during the 2000s in comparison with the previous decade till 2015/2016. Here, we further document the ongoing oceanic changes within the Greenland Sea through the Mercator Ocean Physical System, an operational ocean model with data-assimilation. The model has shown a large variability, a later start and a decline of convection in the Greenland Sea in recent years. In particular, the depth of the annual maximum mixed layer diminished by 52% between 2008–2014 and 2015–2020, from 1,168 to 559 m, over the convective area. This decline of the convection depth is corroborated with Argo float observations. Within the Greenland Sea, hydrographic changes especially the increasing temperature are associated with isopycnal deepening and stratification strengthening. The stratification is building up at a larger rate in the Boreas Basin compared to the Greenland Basin. The changes of the Greenland Sea hydrography in the model are in part related to Atlantic Water spreading over the Boreas Basin and the eastern part of the Greenland Basin. The model also indicates a decrease in the intensity of the gyre in accordance with the isopycnal deepening while local surface winds and fluxes do not exhibit significant trends nor significant interannual variations.

Plain Language Summary Surface warm and salty waters are losing heat as they flow poleward. Once they reach the subpolar Atlantic Ocean, they eventually sink to depth as they are getting denser. This vertical motion is called convection. This is an important process as it contributes to feeding the lower limb of the Atlantic Meridional Overturning Circulation, a key regulator of the global climate. In this study, we investigated wintertime convection evolution in recent years through an ocean model combined with observational data. We focused on the Greenland Sea, a main place regarding convection. The main result is that convection has weakened (in extent and intensity) in recent years. Convection is shallower, covers a smaller area and begins later in the winter. A contributing factor appears to be the rise in oceanic temperature at this location especially near the surface. Therefore it is crucial to keep monitoring this region as this rise in temperature is expected to continue in the future.

1. Introduction

The Nordic Seas (Greenland, Norwegian and Iceland Seas) together with the Fram Strait to the north form an oceanic gateway between the Atlantic and the Arctic Oceans. This area is a place of exchange between several water masses including Polar and Atlantic Waters. The rather cold and fresh Polar Waters leave the Arctic basin near the surface along the east coast of Greenland (Aksenov et al., 2010). The warm and salty Atlantic Waters are the main source of heat and salt for the Arctic Ocean (Schauer et al., 2008). These are carried across from the Nordic Seas at the surface (then subsurface) by the Norwegian Atlantic Current, a two branches current (Orvik & Niiler, 2002). Over the study area, the main circulation pathways are summarized in Figure 1. The latter have been described by numerous authors (e.g., Athanase et al., 2019; Hattermann et al., 2016; Hofmann et al., 2021; Piechura and Walczowski, 1995; von Appen et al., 2016; Walczowski, 2013).

In the middle, the Greenland Sea is a major site of open-ocean convection in winter, a process by which weakened surface stratification facilitates the sinking of surface waters densified by surface cooling, their mixing with underlying layers and the formation of intermediate and bottom waters (Marshall & Schott, 1999). This area is therefore of primary importance regarding the variability of the Atlantic Meridional Overturning Circulation (AMOC), a major component of the global climate, as wintertime convection there contributes to feeding the lower limb

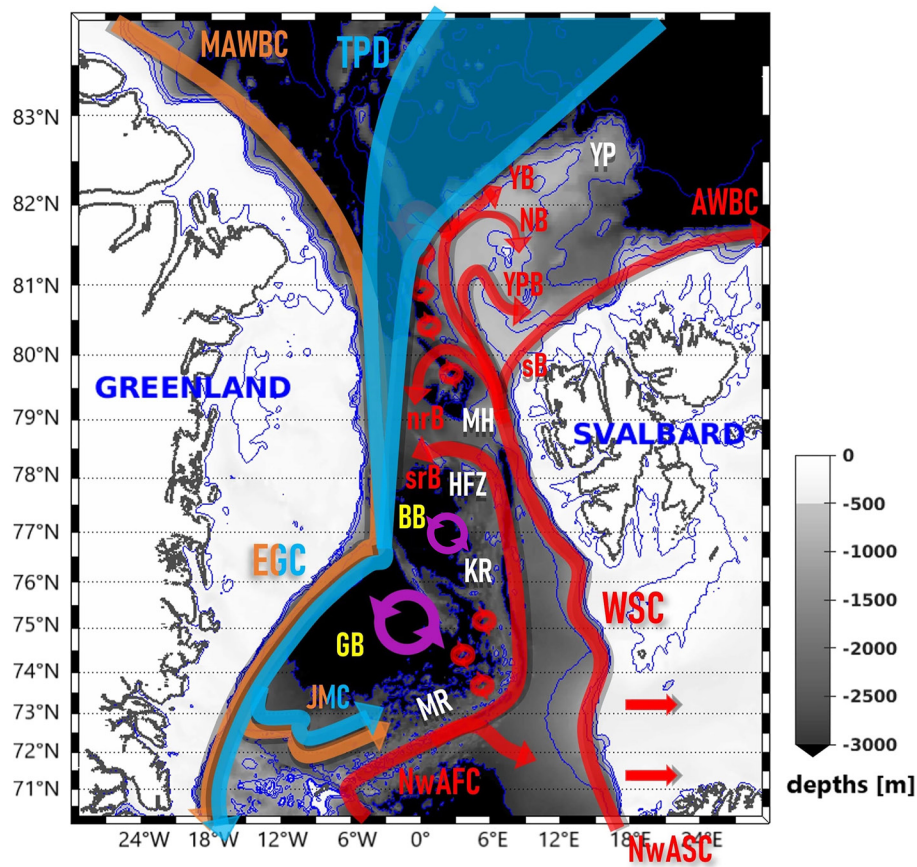

Figure 1. Schematic view of the area (Northern Nordic Seas) and the oceanic circulation. Red arrows account for Atlantic Water, blue for Polar Water and orange for Modified Atlantic Water. The bathymetry is from IBCAO. Dark blue lines are isobaths 100, 500, 700, 1,000, 2,000, 3,000, 3,800 m. Dark contour is the isobath 0m. The main currents are in color, TPD: Transpolar Drift, EGC: East Greenland Current, WSC: West Spitsbergen Current, NwAFC: Norwegian Atlantic Front Current, NwASC: Norwegian Atlantic Slope Current, srB and nrB: southern and northern recirculation Branches, SB: Svalbard Branch, YPB: Yermak Pass Branch, YB: Yermak Branch, NB: Northern Branch, JMC: Jan Mayen Current, AWBC: Atlantic Water Boundary Current and MAWBC: Modified Atlantic Water Boundary Current. The main bathymetric features are in white, MR: Mohn Ridge, KR: Knipovitch Ridge, HFZ: Hovgaard Fracture Zone, MH: Molloy Hole, YP: Yermak Plateau. In yellow, GB: Greenland Basin and BB: Boreas Basin. Purple arrows indicate the Greenland Sea and the Boreas Gyres.

of the AMOC (Huang et al., 2020; Latarius & Quadfasel, 2016). The cyclonic Greenland Sea Gyre favors deep convection as isopycnal doming brings a weakly stratified layer close to the surface (Killworth, 1983). The Greenland Sea encompasses another cyclonic gyre, north of the Greenland Basin, in the Boreas Basin (Quadfasel & Meincke, 1987) also suitable for deep convection to occur. In this basin, convective chimneys of about 3,000 m were observed at the end of March 1989 (SIZEX 89 experiment; Johannessen et al. (1991)). In the Greenland Sea, the deepest mixed layer depths (MLDs) are found in late winter, between February and April (Bashmachnikov et al., 2021; Brakstad et al., 2019).

However, deep convection is not a regular process occurring each winter with the same intensity and it rather exhibits a large interannual variability (Marshall & Schott, 1999). Greenland Sea convection is regulated by numerous factors including surface buoyancy fluxes, intensity of the Greenland Sea Gyre and oceanic heat and salt advection (Bashmachnikov et al., 2021). Convection was very shallow during the 80s in the Greenland Basin (Schlosser et al., 1991). Several authors have mentioned an increase in the wintertime convection intensity during the 2000s, in comparison with the previous decade, linked with a rise of salinity and temperature in the Greenland Sea (Bashmachnikov et al., 2021; Brakstad et al., 2019; Lauvset et al., 2018). All these studies recorded several winters with maximum mixed layers deeper than 1,500 m during the 2000s till 2015/2016. Bashmachnikov et al. (2021) found that the increase in upper layer salinity through Modified Atlantic Water advection from the

West Spitsbergen Current was a primary cause of interannual variability of wintertime convection in the area. Further north, changes in winter mixed layer depths have also been highlighted in recent years. The Yermak Plateau, that used to be ice-covered year-round now experiences occasional ice-free conditions and has repeatedly shown enhanced winter convection over the past decade (Athanase et al., 2020). This northward "shift" of the convection regions has been projected to occur under a warming climate (Bretones et al., 2022; Lique & Thomas, 2018). The ice-edge retreat also contribute to increase air-sea heat fluxes and water mass transformation along the boundary currents in the area (East Greenland Current, West Spitsbergen Current and Svalbard Branch) (Moore et al., 2022; Våge et al., 2018).

In this study, we further document ongoing oceanic changes within the Northern Nordic Seas (Figure 1) taking advantage of the Mercator Ocean operational model which put in a continuous spatio-temporal context the assimilated in situ and satellite data. In Section 2, we briefly present the model and the Argo float data. In Section 3, we examine the evolution of hydrography, circulation and mixed layer depths between 2008 and 2020. Finally, in Section 4 we discuss the contributing mechanisms to the ongoing changes in the Greenland Sea.

2. Material

2.1. Mercator Ocean Operational System (PSY4)

The global operational system Physical SYstem version 4 (PSY4) developed at Mercator Ocean for the Copernicus Marine Environment Monitoring Service (CMEMS; http://marine.copernicus.eu/) simulates ocean physical variables (e.g., temperature, salinity, sea surface height, and velocity) and sea-ice variables from 2007 onward (Lellouche et al., 2018). The physical configuration is based on a 1/12° tripolar grid (Madec & Imbard, 1996) (grid spacing of 4–4.3 km in the Fram Strait region, e.g., Figure 1 in Hu et al. (2019)), with 50 vertical levels of decreasing resolution from 1 m at the surface to 450 m at the seafloor, including 22 levels within the upper 100 m. The PSY4 system uses version 3.1 of the Nucleus for European Modeling of the Ocean model (NEMO; Madec and Engine (2008)) and the Louvain-La-Neuve thermodynamic-dynamic Sea Ice Model (LIM2; Fichefet and Maqueda (1997)). At the surface, the model is driven by atmospheric analyses and forecasts obtained from the European Centre for Medium-Range Weather Forecasts-Integrated Forecast System (ECMWF-IFS) at 3-hr resolution.

The model jointly assimilates along-track satellite altimetry data, satellite sea surface temperature (from Operational Sea Surface Temperature and Ice Analysis, OSTIA), sea-ice concentration (from the Satellite Application Facility on Ocean and Sea Ice, OSI SAF), and in situ temperature and salinity profiles (from the CORA3.3 database) using a reduced-order Kalman filter with a 3-D multivariate modal decomposition of the background error and a 7-day assimilation cycle (Lellouche et al., 2018). During the assimilation procedure, a particular treatment is applied to areas potentially covered with sea ice: all observations errors in the multivariate SEEK filter increase linearly (less weight in the analysis) with the decrease of the SST from −1°C to −1.7°C and the observations are rejected if SST is less than −1.7°C (i.e., an approximation of the freezing point). In other words, apart from the sea-ice concentration no other quantities are assimilated in ice-covered oceans. The model does not include tides and updated runoff climatology is used together with runoff fluxes coming from Greenland (Dai et al., 2009). The PSY4 system starts in October 2006 from a "cold" start (initial currents are null) using initial climatological conditions from EN4.2.1 hydrographic temperature and salinity data (Good et al., 2013). Following Athanase et al. (2021), we considered the first 15 months as a spin up period and used daily fields from January 2008 to May 2020. Absolute salinity SA [g/kg] and conservative temperature CT [°C] are used following the TEOS-10 (Thermodynamic Equations of Seawater) international standard (McDougall & Barker, 2011).

So far, PSY4 evaluations in the upper 600 m of the western Eurasian Basin and northern Fram Strait using non-assimilated data showed that simulated sea-ice cover, temperature, salinity, and ocean currents were in good agreement with observations (e.g., Artana et al., 2022; Athanase et al., 2019, 2020, 2021; Koenig, Provost, Villacieros-Robineau, et al., 2017; Koenig, Provost, Sennechael, et al., 2017). A comparison of a former version of the operational model one fourth degree to in situ data and other models over the Nordic Seas highlighted the system capabilities for reproducing properties in that region (Lien et al., 2016).

2.2. Further Evaluation Over the Northern Nordic Seas

An additional evaluation of the model over the Northern Nordic Seas was performed comparing simulations to Argo float profiles (assimilated by the model) present in the area. There are 7,762 Argo floats profiles from the

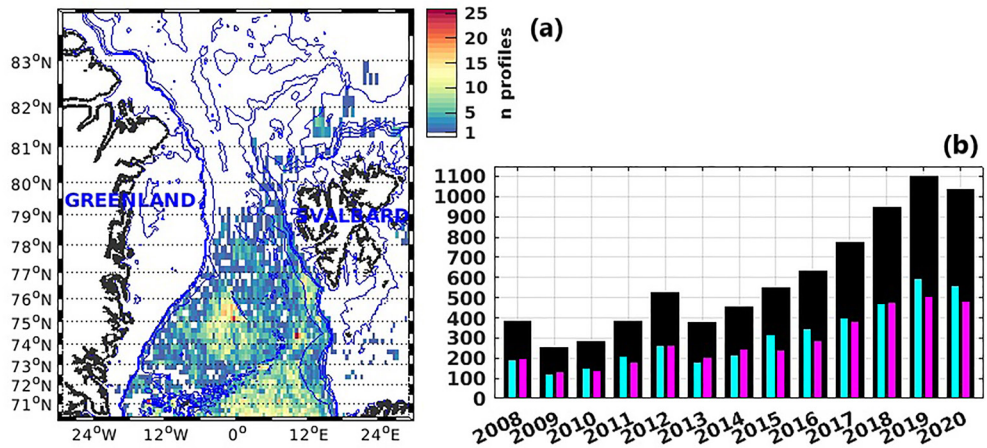

Figure 2. (a) Number of Argo float profiles per 0.5° longitude x 0.25° latitude bin between 70/84°N and −30/30°E during the period 2008–2020. (b) Total number of profiles per year (black bar) and season (color bars). The blue color represents winter months (JFMOND) and the magenta summer months (AMJJAS).

Coriolis data center (only good quality flags are retained) from 2008 to 2020, located between 70 and 84°N and between −30 and 30°E (Figure 2a). The number of profiles increases from 2014 onward, with no seasonal bias (Figure 2b). Highest profile densities are found in the center of the Greenland Sea Gyre and east of the Mohn and Knipovitch Ridges; there are very few profiles north of 79°N because of sea ice (Figure 2a).

Daily PSY4 fields were colocated in time and space (closest grid cell) with the in situ profiles. Profiles from PSY4 modeled data were linearly interpolated to 1 m vertical resolution to ease model-observations comparisons. Correlations between PSY4 colocated variables and observed data is 0.98 for temperature and 0.93 for salinity (both are statistically significant to the 99% confidence level). Conservative temperature and absolute salinity diagrams with data plotted chronologically from 2008 to 2020, highlight a striking freshening of the water column in both observations and model (shift toward lower salinity values above isopycnal 28.1 kg/m^3 in Figures 3a and 3b). This is consistent with the freshening of the upstream Norwegian Sea (around 65°N) during the 2011–2018 period reported by Mork et al. (2019).

Maps of hydrographic properties were derived by averaging data of all available profiles in square bins of 0.5° longitude × 0.25° latitude. The same was performed with the PSY4 colocated data for comparison. We examined both the 25 and 222 m depth horizons, levels that rather well depict the near surface and the Atlantic Water respectively. In the following, biases are defined as the mean of absolute differences between the model and the observations over late winter months (JFMA; convective period). During this period, biases are relatively small.

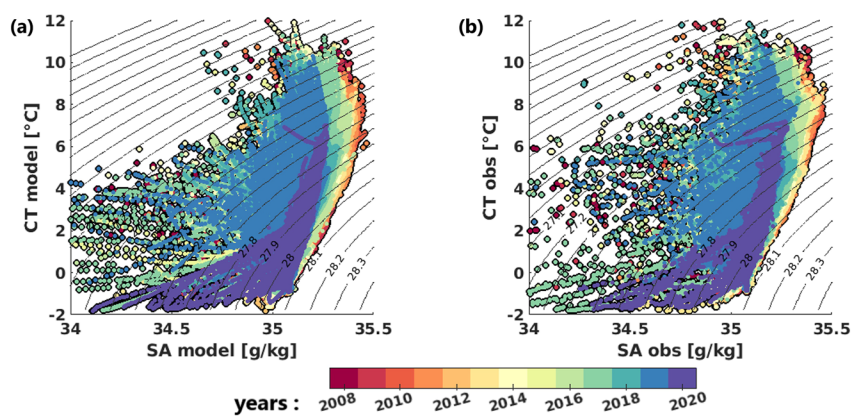

Figure 3. CT-SA diagram from (a) PSY4 colocated and (b) observed conservative temperature and absolute salinity during 2008–2020. 6,358 Argo profiles between −10/15°E and 70/79°N from January 2008 to May 2020 were used. Profiles are displayed chronologically from 2008 to 2020.

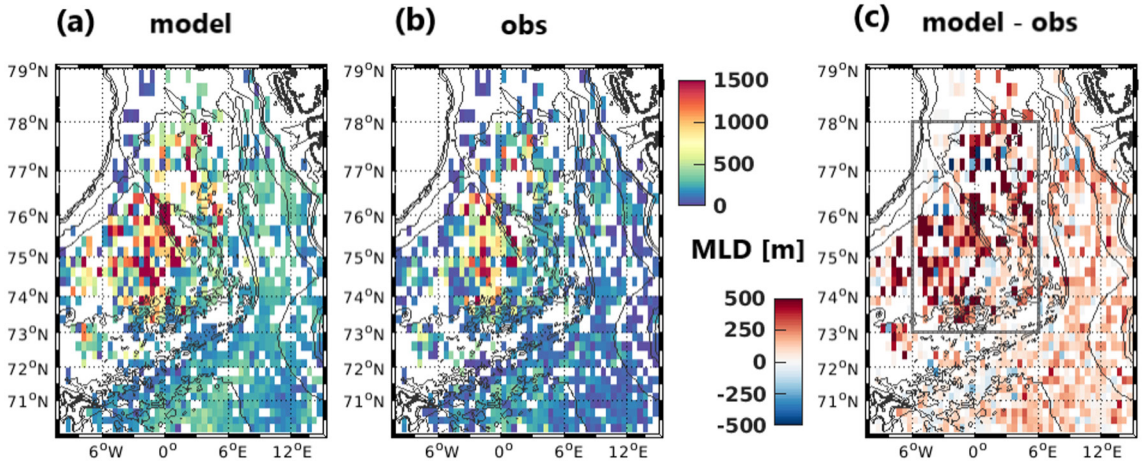

Figure 4. Mixed Layer Depths for JFMA months averaged per bin of 0.5° × 0.25° longitude × latitude from (a) PSY4 colocated, (b) Argo float observation and (c) the difference. 1936 Argo profiles between −10/15°E and 70/79°N during 2008–2020 in JFMA were used.

At 222 m (Figure S1 in Supporting Information S1), biases are of about 0.40°C for conservative temperature and 0.02 g/kg for absolute salinity (RMSE are 0.62°C and 0.03 g/kg) with the largest differences along the Mohn and Knipovitch Ridges in the frontal zone. Near the surface (Figure S2 in Supporting Information S1), biases are 0.51°C for conservative temperature and 0.04 g/kg for absolute salinity (RMSE are 0.82°C and 0.08 g/kg) with the modeled surface being slightly colder and saltier over the Greenland Sea.

We then compared mixed layer depths in winter months (Figure 4). MLDs were computed from a density-based criterion, that is, the mixed layer depth is the depth d verifying $\sigma(d) = \sigma(10\text{m}) + \delta\sigma$, with σ the potential density referenced to the sea surface and $\delta\sigma = 0.01$ kg/m^3. The main convection sites (in the Greenland and the Boreas Basins) are rather well located in the model (Figures 4a and 4b). However the model overestimates MLDs: the mean MLD bias over the entire area is about 196 m (RMSE is 330 m) and it is about 311 m (RMSE is 490 m) inside the convection region (gray contour; Figure 4c). This could be due to a combination of slight negative (resp. positive) biases in temperature (resp. salinity) near the surface (Figure S2 in Supporting Information S1) and to the model decreasing vertical resolution with depth (450 m at the seafloor).

At the location of the largest MLD biases (gray contour; Figure 4c), we further examined Argo profiles in CT, SA as well as derived density and buoyancy frequency squared and their colocated variables in the model (Figure 5). Temporal evolution of these physical quantities is well reproduced by the model. Similar patterns are found in both the Argo profiles and the model outputs over the period. These include for example, a density decrease and temperature increase in the upper layers comparing the last years with the beginning of the period (Figure 5a,5b), a salinity increase between 500 and 2,000 m (Figure 5c), a stratification increase over the entire water column (Figure 5d). Note that the colorbar we used for the buoyancy frequency squared, similar to Brakstad et al. (2019) is not a linear one. Regarding MLDs, correlations between PSY4 colocated and Argo derived MLDs is 0.71 (statistically significant above the 99% confidence level) and correlation of JFMA means is even larger: 0.89 (statistically significant above the 99% confidence level; Figure 5e).

Overall, the model reproduces well the hydrographic properties and the temporal evolution of the winter mixed layer depths ($r = 0.89$) despite an overestimation. Before investigating variations in winter MLDs, we looked into linear trends in hydrography and circulation although linear trends do not depict the full story.

3. Low Frequency Evolution of the Northern Nordic Seas Over 2008–2020

3.1. Linear Trends in Hydrography and Circulation in the Northern Nordic Seas

Means and trends are shown at 25 and 222 m depth horizons, levels that rather well depict the surface and the Atlantic Water respectively (Figures 6 and 7). Means are shown as a reference to ease the interpretation of trends (in units per decade). Near the surface, temperature has increased north of Svalbard over the Yermak Plateau and in the Atlantic Water Boundary Current (Figure 6b) which is consistent with the northward progression and shoaling of Atlantic Water (AW) in the Arctic (e.g., Polyakov et al., 2017; Athanase et al., 2021). In the

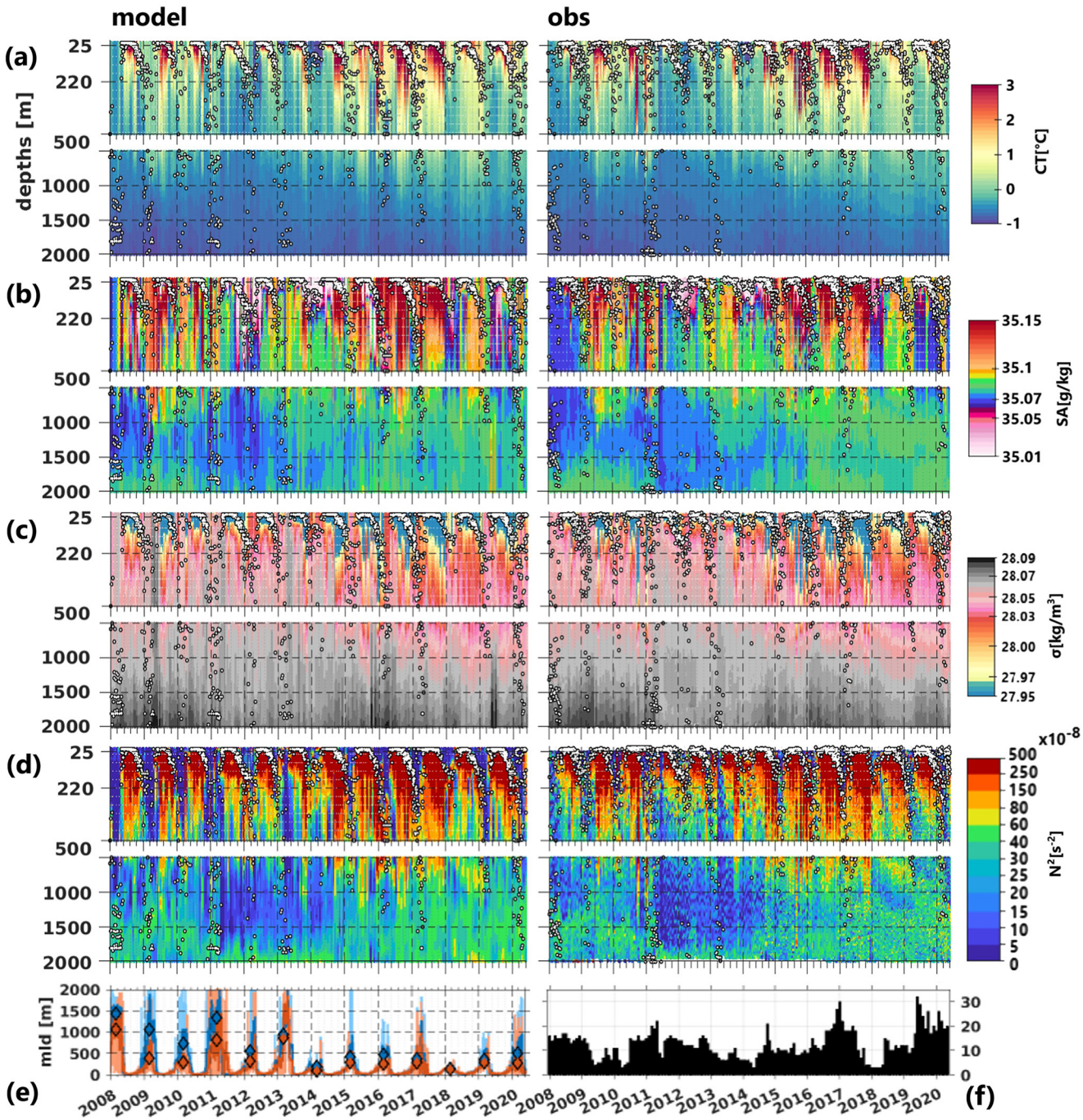

Figure 5. Individual profiles within the box defined by 73/78°N and −6/6°E (gray contour; Figure 4c) from (left column) PSY4 variables colocated in time and space with observations and (right column) Argo float profiles as a function of time. (a) Conservative temperature [°C], (b) absolute salinity [g/kg], (c) density [kg/m^3] and (d) buoyancy frequency squared (N^2) [s^{-2}]. Dots in the left column are the PSY4 colocated MLDs and dots in the right column are MLDs derived from the observations. (e) MLDs from (pale blue) PSY4 colocated data and (pale orange) Argo, bold blue and orange are associated 5 days running means and diamonds are JFMA means. (f) Monthly Argo float distribution over years within the same box (there is a total of 1,871 profiles).

Greenland Sea, west of the Knipovich Ridge, temperature also increased by about +1°C/dec. Interestingly, there is no significant temperature trend in the West Spitsbergen Current (WSC). North of 80°N, salinity strongly increased (>+0.6 g/kg/decade; Figure 6d) along the Greenland slope and north of the Yermak Plateau. This is consistent with the reduction in Arctic's freshwater outflows through Fram Strait between 2008-2014 and 2015–2020 (Bertosio et al., 2022; Karpouzoglou et al., 2022).

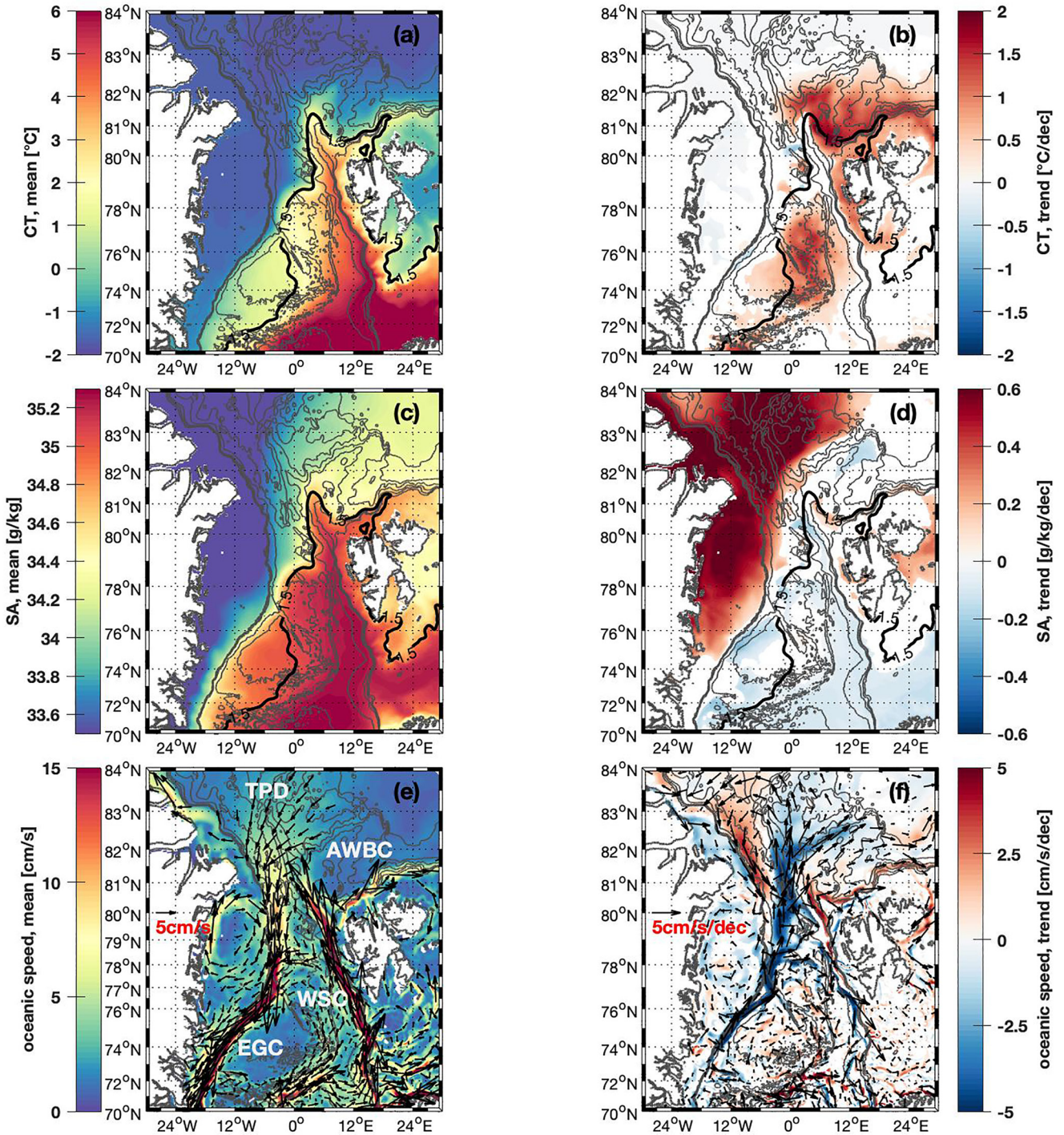

Figure 6. Means and trends over 2008–2020 at 25 m depth horizon. (a) Mean conservative temperature [°C] and (c) absolute salinity [g/kg] and associated linear trends (b) in [°C/dec] and (d) in [g/kg/dec]. Dark bold contour is the mean 1.5°C isotherm over 2008–2020. 25 m (e) mean oceanic circulation [cm/s]. Black arrows correspond to the mean current and background color is speed. (f) Associated linear trends [cm/s/dec]. Background color is the trend of the norm and black arrows are the resultant of the meridional and zonal component trends. Retained values for trends calculation are such that $|nt.\frac{slope}{std}| > 1$, with nt the number of points used to calculate the regression (*slope*) and the standard deviation (*std*).

South of 80°N, surface velocities of the East Greenland Current (EGC) have decreased with a trend of about −5 cm/s/decade (Figure 6f). The latter is consistent with the observed EGC slowdown at 78°50′N after 2015 which was partly related to a salinity increase in the lower halocline over the shelf (Karpouzoglou et al., 2022).

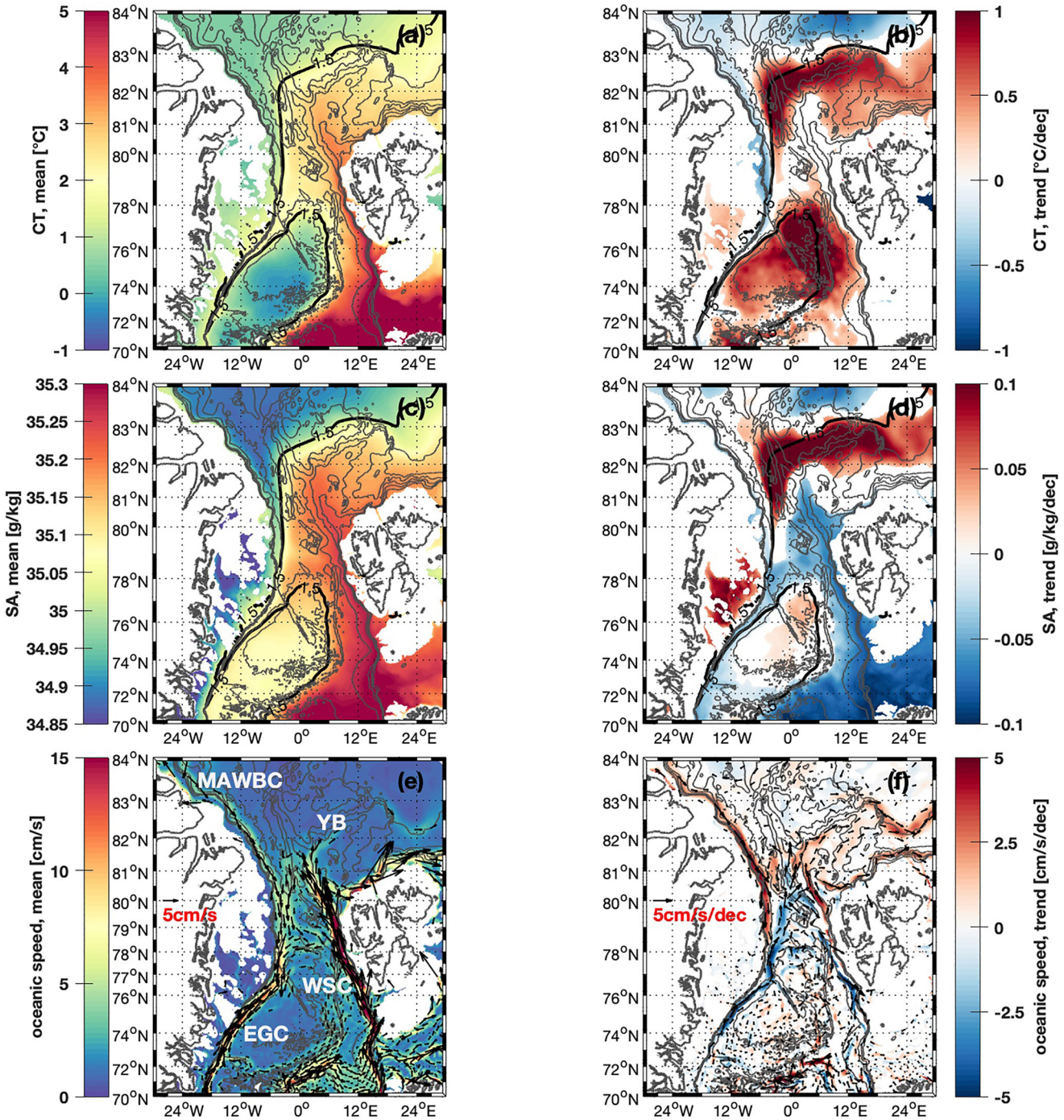

Figure 7. Means and trends over 2008–2020 at 222 m. (a) Mean conservative temperature [°C] over 2008–2020 and (c) absolute salinity [g/kg] and associated linear trends (b) in [°C/dec] and (d) [g/kg/dec]. Dark bold contour is the mean location of 1.5°C isotherm over 2008–2020. 222 m (e) mean oceanic circulation [cm/s] over 2008–2020. Black arrows correspond to the mean current direction and color the oceanic speed. (f) Associated linear trends [cm/s/dec]. Background color is the trend of the norm and black arrows are the resultant of the meridional and zonal component trends. Retained values for trends calculation are such that $|nt.\frac{slope}{std}| > 1$, with nt the number of points used to calculate the regression (*slope*) and the standard deviation (*std*).

At 222 m, hydrography and circulation patterns also display systematic trends that do not necessarily follow the surface ones (Figures 6 and 7). In the north, surroundings of the Yermak Plateau show a strong increase in temperature (>+1°C/decade) and salinity (>+0.1 g/kg/decade) (Figures 7b and 7d). The latter are associated with intensified velocities along the western flank of the Yermak Plateau, the northward shift of the location of

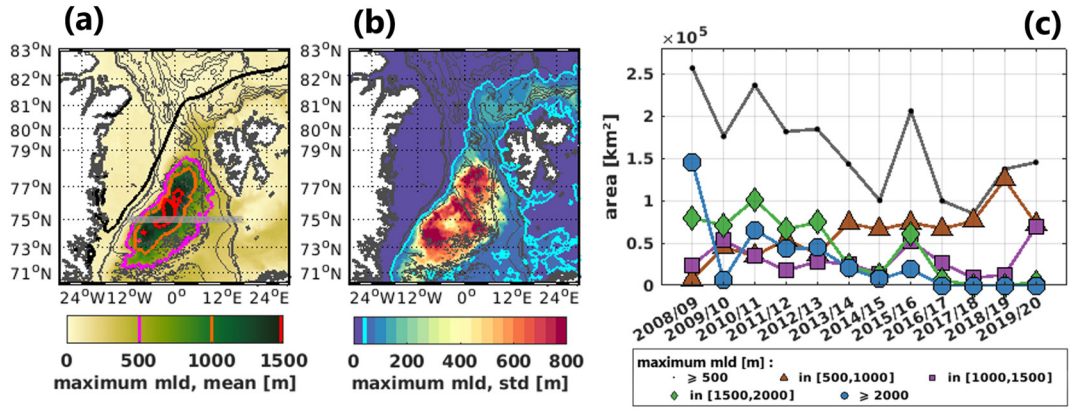

Figure 8. (a) Annual maximum Mixed Layer Depth [*m*] averaged over 2008–2020. Black contour is the mean ONDJFM 80% ice-edge. Pink, orange and red contours are the 500-, 1,000- and 1,500 m mMLD-isocontours. (b) Associated standard deviation. Cyan contour is the 40 m std-isocontour. (c) Area [km^2] with maximum Mixed Layer Depth between 500 and 1,000 m (orange), 1,000 and 1,500 m (purple), 1,500 and 2,000 m (green) and larger than 1,500 m (blue) as a function of time (year). Properties along the gray section in panel (a) are shown in Figure 11.

AW recirculation branches and the developing V-shaped circulation north of Svalbard documented by Athanase et al. (2021). Linear trends in temperature and salinity are also positive in the Greenland Sea (>+1°C/decade and >+0.04 g/kg/decade). This could be related to the spreading of Atlantic Water from the Knipovich Ridge toward the Greenland Sea as discussed in Section 4.2. Further east, along the Atlantic Water pathway, the salinity trend is negative (<−0.05 g/kg/decade). This might be related to a freshening anomaly in the subpolar North Atlantic for the period 2012–2016 reported by Holliday et al. (2020). According to the authors, it takes 4–6 years for such an anomaly to reach the Fram Strait. Thus the negative trend could be a signal of this freshening event.

Atlantic Water recirculation velocities between 78°N and 80°N have diminished slightly (Figures 6f and 7f). This could contribute to the velocities weakening of the downstream EGC (<−2 cm/s/decade; Figure 7f). Interestingly, the model also shows an intensification of the Modified Atlantic Water Boundary Current (north of 78°N) velocities at depth (>+2 cm/s/decade; Figure 7f).

3.2. Changes in Winter Mixed Layer Depths

We considered periods ranging from 1 June to 31 May of the following year to avoid splitting winters in two. For each period, we derived maximum Mixed Layer Depth (mMLD) from monthly outputs to quantify winter convection. The main convection zone is located in the Greenland Sea, from the Hovgaard Fracture Zone to the Jan Mayen Island (Figure 8a). It comprises two basins: the Boreas Basin (BB) to the north and the Greenland Basin (GB) to the south. In the following, when no other indications, the term "convective area" refers to the interior of the mean position of the 500 m mMLD isocontour (pink in Figure 8a).

The standard deviation in mMLDs shows a striking maximum (>800 m) in the Greenland Sea, highlighting large interannual variability (Figure 8b). There, the area with the deepest mixed layers (>1,500 m; green and blue curves in Figure 8c) decreases drastically (from a maximum of $2.25 \cdot 10^5$ km^2 in 2008/2009) and is nearly one hundred times smaller after winter 2016/2017 ($2.43 \cdot 10^3$ km^2 between winter 2016/2017 and 2019/2020). In contrast, the area of moderated mixed layer depths (between 500 and 1,000 m; orange curve in Figure 8c) increases in the convection zone and nearly doubles between the beginning and the end of the period. Year 2019/2020 shows a maximum of the area associated with mMLD between 1,000 and 1,500 m while the total area covered with mMLD larger than 500 m (145,010 km^2) is relatively small in comparison with the beginning of the period. This suggests that the convection zone was constrained in a narrow region for this period. Indeed, over the entire convection zone the area covered with mMLDs larger than 500 m (black curve in Figure 8c) decreases throughout the period from 212,300 km^2 between 2008/2009 and 2011/2012 to 116,530 km^2 between 2016/2017 and 2019/2020 (−45%) with a recovery in 2015/2016 of 205,660 km^2 (Figure 8c). This is consistent with the reduction in the deep MLDs area observed in Argo float data for different periods (Figure S3 in Supporting Information S1).

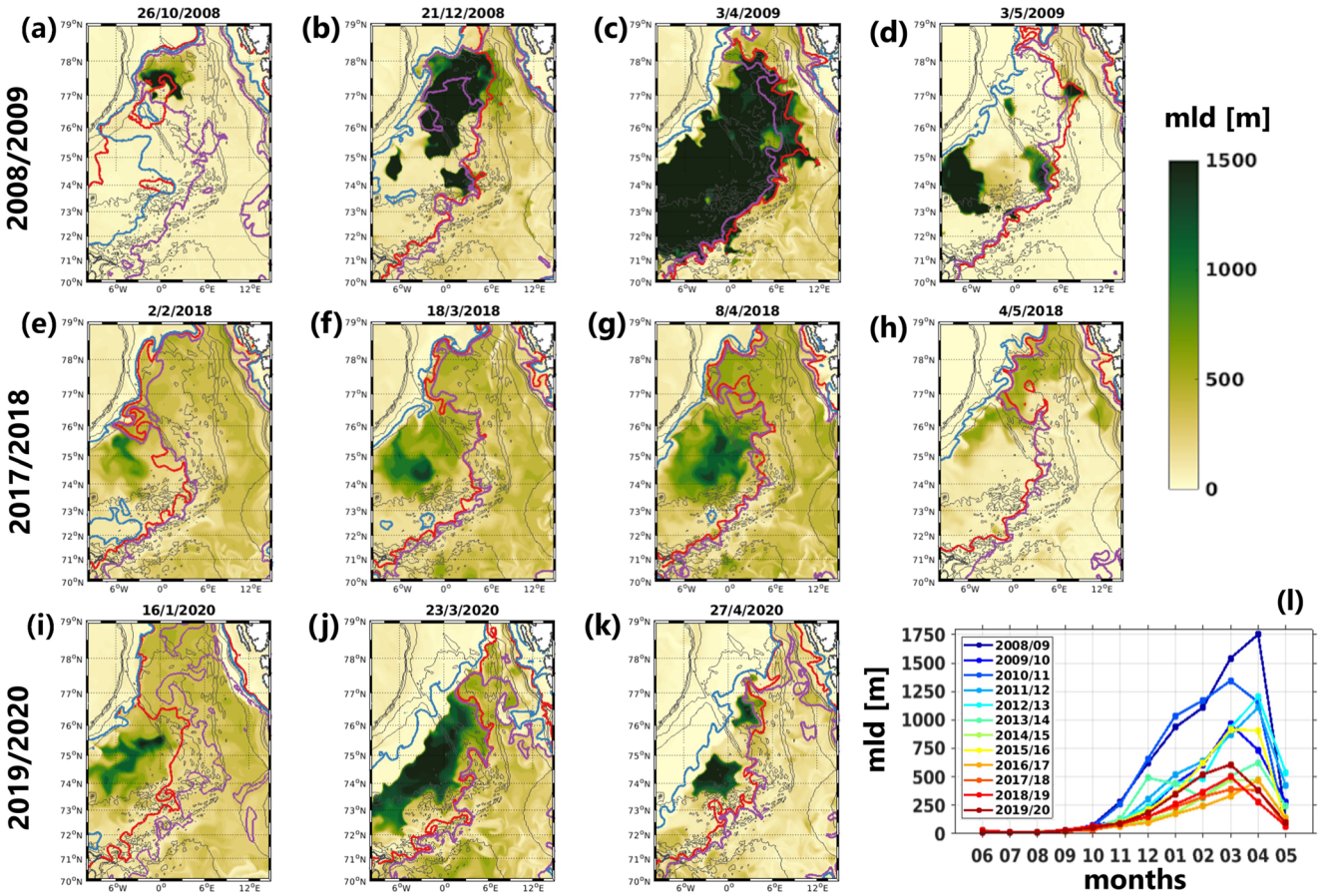

Figure 9. Snapshots of modeled Mixed Layers Depths for three winters: (a–d) 2008/2009, (e–h) 2017/2018; and (i–k) 2019/2020. Red contour is the 1.5°C isotherm, blue and purple contours are respectively the 34.92 and 35.15 g/kg isohalines at 25 m. Note that the dates are not the same for each winter, they have been chosen to illustrate the beginning, the middle and the end of the convection period. (l) Monthly mean MLDs within the 500 mMLD isocontour (pink in Figure 8a). Note that years are defined as period ranging from June to May.

To summarize, the model indicates a convection decline in the Greenland Sea: in intensity (decrease in the total area with mMLDs larger than 1,500–2,000 m) and in extent (decrease in the total area with mMLDs larger than 500 m) in recent years. These results are supported by the observations (Figure 5e and Figure S3 in Supporting Information S1).

3.3. Convection Study Cases: Winters 2008/2009–2017/2018–2019/2020

To describe MLD changes more precisely, we examined their daily evolution during each winter. Below, three specific ones are described: winter 2008/09 and winter 2017/18 which features respectively the largest and the smallest area with mMLDs larger than 500 m (black curve in Figure 8c) and winter 2019/20 which displays a recovery of this same area.

In winter 2008/09, deep convection (MLD > 1,500 m) starts at the end of October 2008 north of the area in the Boreas Basin (Figure 9a). The convective region remains in the Boreas Basin and widens to the south throughout the entire winter till the end of April. Two other convective zones develop further south in late November and mid-December (Figure 9b). At the beginning of February, all the patches have merged (Figure 9c). Mid-February another patch opens north of the Jan Mayen Island. All the patches merged in the beginning of March to form a convective area covering the entire Greenland Sea (Figure 9c). The convection decreases rapidly at the end of April and stops completely by mid-May with the restratification of the water column.

Winter 2017/2018 is far different with a later start of the convection process (in February) in the center of the Greenland Basin (Figure 9e). Convection deepens in the center of the gyre and never reaches 1,500 m (Figures 9f and 9g). Convection declines in the middle of April and restratification occurs in May (Figure 9h).

In winter 2019/20, convection starts in the beginning of January 2020 in the central Greenland Sea (Figure 9i). This winter features mixed layers deeper than 1,500 m which are first localized in the center of the Greenland Sea Gyre. The main convection region extends from the GB to the BB, between the low and high surface salinity waters until mid-April (Figure 9j). Between mid-March and mid-April, the convection process is intermittent with several stops and starts (Figure 9k). It stops definitively by mid-May.

The model suggests that deep winter convection occurs in the Boreas Basin (Figures 5 and 9) where a small cyclonic gyre has previously been observed (Quadfasel & Meincke, 1987). Winter convection has been documented in the 1980's in the Boreas Basin (e.g., Johannessen et al., 1991; Johannessen and Lygre, 1996) and is detectable in Argo float data during 2008–2020 (Figure 4b). The model also indicates that the deepest mixed layers are formed later in winter in recent years and that the convection period is getting shorter. Indeed, defining the beginning of deep convection as the date at which 10 grid points have MLDs larger than 1,000 m, convection starts in October, November or December for most winters but in January for winter 2019/20, February for winters 2014/2015, 2017/2018, and 2018/2019 and in March for winter 2016/2017. Considering the end of convection as the last date with 10 grid points with MLDs larger than 1,000 m, convection period lasts more than 180 days (∼6 months) until 2013/2014 and then diminishes with minima of 69 and 70 days in winters 2017/2018 and 2018/2019. Moreover, monthly mean mixed layer depths within the convection zone shows a shortening of the convection period (Figure 9l). For example, in 2008/2009 MLDs reaches 250 m in late November while in 2018/2019 this depth is reached in January. This result is difficult to corroborate with the observational data since they do not provide continuous spatial and temporal coverage. However, none of the Argo data show an early convection in recent years.

3.4. Stratification Changes in the Greenland Sea

To characterize water properties within the convective area, we averaged physical quantities (density, temperature, salinity and buoyancy frequency squared) over the water column down to 2,000 m within the mean 500 m mMLD isocontour (pink in Figure 8a). The resulting time series are shown in Figure 10. The same time series were produced distinguishing the Boreas and the Greenland Basin and are shown in Supporting Information S1 (Figure S4). We also introduce convection resistance (CR) which measures the amount of buoyancy that must be removed for the water column to mix down to 1,000 m, we adapted the definition of Frajka-Williams et al. (2014) as follows:

$$CR(h) = h.\sigma_1(SA, CT, h) - \int_{-h}^{0} \sigma_1(SA, CT, z)dz \quad (1)$$

with h = 1,000 m and σ_1 the density anomaly referenced to 1,000 m. Thus more positive values indicate stronger stratification; negative values indicate an unstable water column while a well-mixed water column has a convection resistance close to zero.

Winter mixed layer depths have been decreasing during the 2010s' inside the convection zone (Figure 10a). The annual maximum declines from 1,168 ± 375 m (mean ± std) between June 2008 and May 2014 to 559 ± 184 m between June 2014 and May 2020 (−52%) (Figure 10a). MLDs of the Boreas Basin are quite similar to those of the Greenland Basin with associated annual mMLDs only exceeding 1,000 m before 2013 (Figure S4 in Supporting Information S1). One exception is the large winter convection occurring only in the Greenland Basin in early 2016.

Over the period, as upper waters get warmer (Figures 6 and 7b), isopycnals deepens (Figures 10a and 10b). For example, the 28.05 kg/m^3 isopycnal (the light pink contour in Figure 10a) mostly lies above 500 m until 2014 and even goes up to the surface during some winters. After 2015, it never goes to the surface anymore and mostly remains deeper than 500 m. This isopycnal deepening takes place together with a temperature increase that is significant for all season over the entire water column. Here again, taking an example, the 0.2°C isotherm never goes up to the surface after 2014 and remains below 400 m (Figure 10b). Near the surface, salinity does not exhibit clear low frequency changes over the convective area nor specific interannual fluctuations matching the MLD variations (Figures 6d and 10c). For all season, absolute salinity trends are only significant below 700 m where they are positive. At 1,000 m for instance, salinity trend is about +0.008 g/kg/decade over the period. There, salinity increases till 2015 and remains relatively stable after, from 35.074 g/kg between 2008 and 2013 to 35.079 g/kg after.

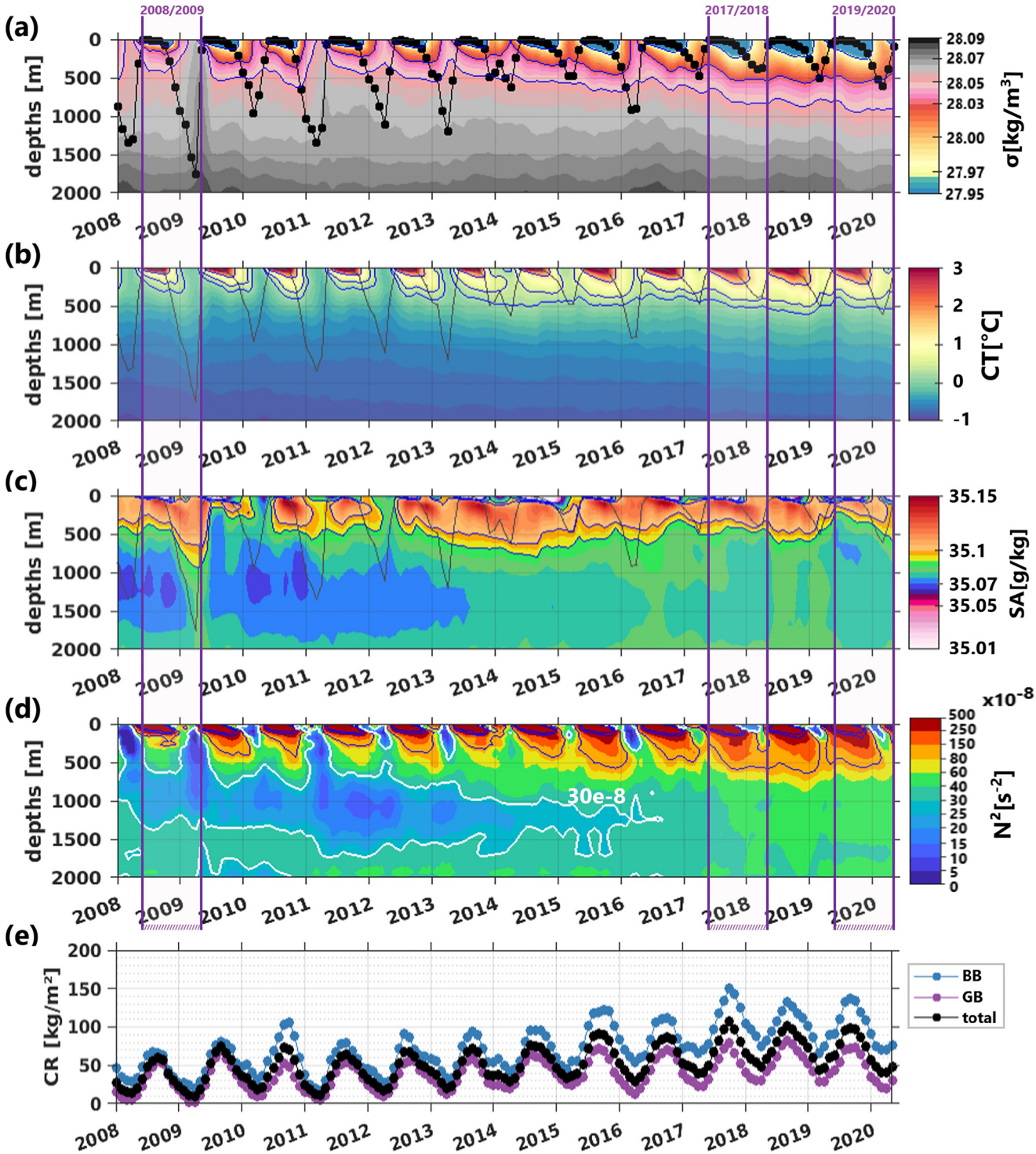

Figure 10. Water Properties averaged within the convection zone (500 m MLD-isocontour, pink in Figure 8a) as a function of time. (a) Density [kg/m^3]. Black dots is the temporal evolution of monthly MLD averaged in the same area. (b) Conservative temperature [°C], (c) absolute salinity [g/kg] and (d) buoyancy frequency squared (N^2) [s^{-1}] averaged in the same area. Blue lines are respectively isopycnals 27.97, 28.03, and 28.05; isotherms 0.2, 0.5, and 1.5; isohalines 35.05, 35.09, and 35.1; iso-N^2 $100 \cdot 10^{-8}$, $500 \cdot 10^{-8}$ and $800 \cdot 10^{-8}$. White line in (d) is the $30 \cdot 10^{-8}$ value. (e) Convection Resistance [kg/m^2] averaged within (black) the convection zone, (blue) the Boreas Basin and (purple) the Greenland Basin.

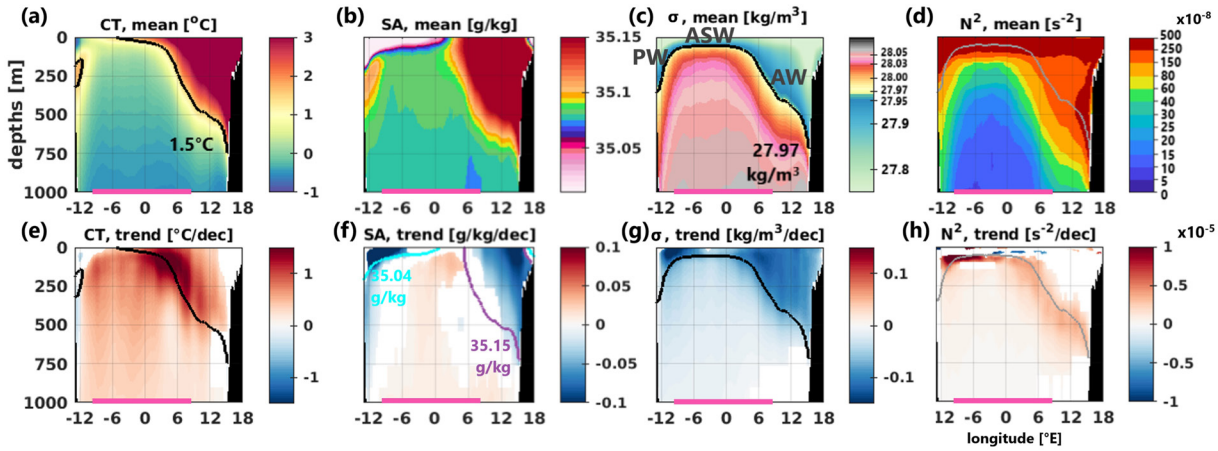

Figure 11. Hydrographic variables along Section 75°N over 2008–2020. (a) Mean conservative temperature [°C], (b) absolute salinity [g/kg], (c) density [kg/m^3] and (d) buoyancy frequency squared (N^2) [s^{-2}]. (e), (f), (g) and (h) are associated linear decadal trends. Black contour in (a, e) is the mean 1.5°C isotherm, cyan and purple contours in (b,f) are those of the 34.92 and 35.15 g/kg isohalines, black and gray contours in (c, d, g, h) mark the 27.97 kg/m^3 isopycnal. Pink color on the longitude-axis is the overlap with the convective area (pink contour, Figure 10).

Hydrographic changes led to a stratification strengthening above 2000 m (Figure 10d). Over the entire convection zone, the early winter (OND) stratification of the first 500 m is associated with N^2 of about 304.10^{-8} s^{-2} for the four first years and 525.10^{-8} s^{-2} for the four last ones (+73%). The weakly stratified water reservoir (within the white contour in Figure 10d) that is replenished during convective events has faded over the 2008–2020 period. After 2013/2014 the reservoir no longer replenishes and disappears after 2016. The above mentioned changes are consistent with the discrete profiles shown in Figure 5.

The decrease in winter mixed layer depths during the 2010s is consistent with the increase in convection resistance within the convection zone, the associated trend is about +36 kg/m^2/decade (Figure 10e). For comparison, the trend in convection resistance calculated from the available Argo profiles in the same area and averaged for each month is about +31 kg/m^2/decade (Figure S5 in Supporting Information S1). Both are significant according to the criteria $|nt.\frac{slope}{std}| > 1$, with *nt* the number of points used to calculate the regression *slope* and the standard deviation *std*. Both basins exhibit positive convection resistance trend and convection resistance is always closer to zero in the Greenland Basin than in the Boreas Basin (Figure 10e and Figure S5 in Supporting Information S1, purple and blue lines, respectively). In comparison with the Greenland Basin, the trend is larger in the Boreas Basin (56 kg/m^2/decade in the model, significant). This means that upper layers are becoming more stratified with a larger rate of change for the Boreas Basin in comparison with the Greenland Basin.

4. Discussion

4.1. Influence of Temperature and Salinity Variations on Stratification Changes

The zonal section at 75°N (blue line in Figure 8a) illustrates means and trends of hydrographic properties in the Greenland Sea. The 27.97 kg/m^3 isopycnal (black contour in Figure 11c) distinguishes upper layers from intermediate ones. Upper layer thus includes Arctic Surface Water (ASW) in the central part, Polar Water (PW) on the western side and Atlantic Water (AW) along the eastern rim (Figure 11c). Intermediate layer includes Greenland Sea Intermediate Water, Modified Atlantic Water and dense Atlantic Water (X. Wang et al., 2021).

Trends are positive (resp. negative) in temperature (resp. in density) throughout the upper 1,000 m and change sign in salinity around the depth of the 27.97 kg/m^3 isopycnal (Figures 11e–11g). Temperature trends are larger than +1°C/decade and salinity trends are smaller than −0.1 g/kg/decade in the upper layer. Both are driving a density decrease of about −0.09 kg/m^3/decade in the upper layer. In the intermediate layer, both temperature and salinity trends (about 0.5°C/decade and 0.005–0.02 g/kg/decade) are positive and significant. The overall density decrease of about −0.01 kg/m^3/decade in the intermediate layer shows that the temperature effect on density dominates. To summarize, density variations are larger in the upper layer than in the intermediate one and lead to an increase in the vertical density gradient and in the stratification between the two layers along the 75°N section (Figures 11d and 11h).

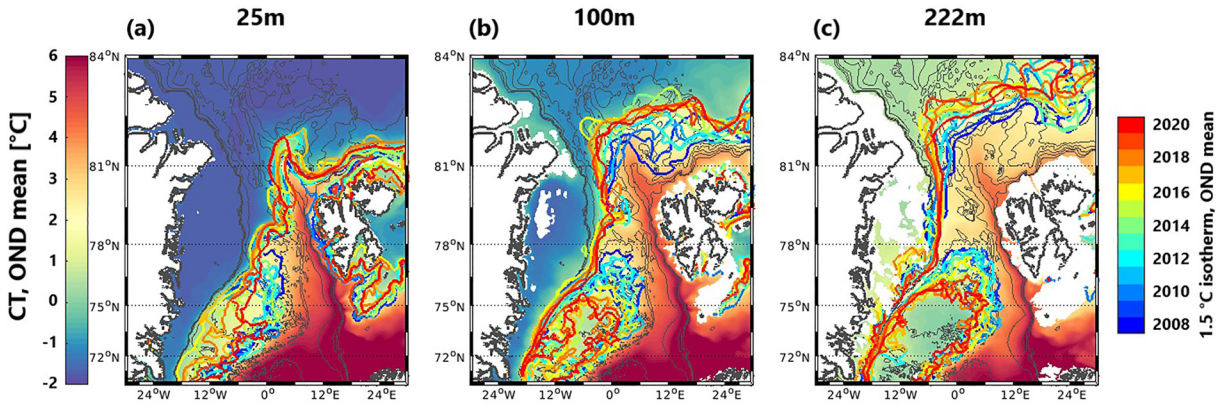

Figure 12. Contours of the 1.5°C isotherm at (a) 25 m, (b) 100 m, and (c) 222 m averaged over the pre-convective period (OND) from 2008 to 2020. Contour color follow the year colorbar (on the right). Background maps are OND means during the entire period.

4.2. Atlantic Water Spreading Into the Greenland Sea

A possible contributor to the stratification changes in the Greenland Sea is the Atlantic Water spreading into the Greenland Sea (e.g., Årthun et al., 2019; Bashmachnikov et al., 2021). To illustrate the Atlantic Water spreading, we show the mean 1.5°C isotherm for the pre-convective period (OND) of each year at three different depths (Figure 12).

The mean isotherm moves toward the central Greenland Sea with years, from the Hovgaard Fracture Zone and the Knipovich Ridge. At the end of the study period, the Atlantic Water layer covers the Boreas Basin. The latter is in good agreement with positive temperature and salinity trends at 222 m over the Boreas Basin in Figures 7b and 7d.

Horizontal velocities does not exhibit significant trends in the Atlantic Water layer between 70 and 78°N (Figures 6 and 7e, 7f). The Atlantic Water layer expansion and thus the heat increase in the Greenland Sea gyre could result from a combination of both Atlantic Water changing properties and increasing exchange through mesoscale activity. Indeed, the model shows a positive eddy kinetic energy (EKE) trend along the Mohn and Knipovich Ridges with an activation from 2015 onward as well as increased eddy heat transfer into the Greenland Sea upper layers (Figure S6 in Supporting Information S1). The Atlantic Water layer expansion toward the interior during the pre-convective period might inhibit convection in a first place, as it results in a more stratified environment (Figures 10d and 10e and 11).

4.3. Gyre Circulation

In addition to the hydrographic changes above-mentioned, we examined the evolution of the Greenland Sea cyclonic gyre. Indeed, a weakening of the gyre (less cyclonic) would lead to isopycnal deepening. In order to quantify the gyre intensity, we derived a gyre index as in Chatterjee et al. (2018). We first computed the vertically integrated (from the surface to the bottom) transport stream function. The latter was then averaged inside box 73/78°N and −12/9°E, over the regions deeper than 3,000 m (black area in Figure 1) to obtain the index.

The index shows a large seasonal cycle and interannual variability. The index trend over the entire period is negative and of about −0.14 Sv/year (significant). The decrease rate is larger after 2015 (−0.60 Sv/year) (Figure 13). The weakening of the gyre could contribute to the convection decline over the Greenland Sea in recent years.

4.4. Local Atmospheric Forcing

We also investigated local surface winds and fluxes from ERA5 reanalysis (Figure S7 in Supporting Information S1). Surface winds and fluxes do not exhibit neither significant trends nor significant interannual variations. We paid particular attention to winter turbulent heat fluxes following Moore et al. (2015) who showed that sea-ice retreat over the Greenland Sea led to reduced fluxes implying a decrease in winter convection. Winter (NDJFMA) turbulent heat fluxes over the gyre (again inside the pink contour in Figure 8a), show no particular trend during 2008–2020 (Figure S7d in Supporting Information S1). The extreme values are reached in winter

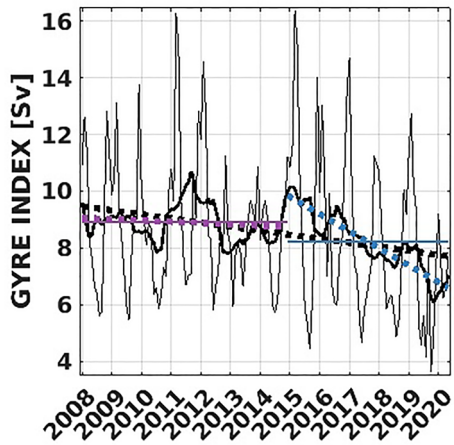

Figure 13. Monthly gyre index time series, 12-month running mean (dark bold), computed as in Chatterjee et al. (2018) by taking the averaged barotropic stream function inside the 3,000 m isobath in box 73/78°N−−12/9°E, over the 2008–2020 period. Thin purple and cyan lines are means. Linear trends are indicated with dotted lines.

2019/2020 (−176 W/m^2; maximum in absolute value) and winter 2013/2014 (−110 W/m^2; minimum in absolute value) in comparison with the mean value of −132 W/m^2. However, these are not associated with extreme MLD values as the fluxes did not manage to break the stratification (Figures S7a and S7d in Supporting Information S1).

5. Summary and Concluding Remarks

We examined the evolution of wintertime convection over the Greenland Sea between 2008 and 2020 through the Mercator Ocean Physical System (PSY4). The model showed a good ability in depicting the Northern Nordic Seas hydrographic properties over the period (Figure 5). Although model Mixed Layer Depths (MLDs) in the JFMA (during the convection period) are positively biased, their temporal evolution is well represented and the correlation coefficient between modeled and observed MLDs in winter within the convective area is of 0.89 (Figures 4 and 5).

The model documents a large variability of winter convection in the Greenland Sea, both in the Greenland and Boreas Basins. The main results are as follows:

1. The maximum depth of deep convection decreased in recent years (Figures 5e, 8c, and 10a). Within the convective area, the maximum of averaged mixed layer depth reduced by 52% between 2008–2014 and 2015–2020 from 1,168 ± 375 m to 559 ± 184 m (Figure 10a).
2. The extent of deep convection decreased in recent years (Figure 8). The area with mMLDs >500 m reduced by 45% comparing the beginning and the end of the period, between 2008–2012 and 2016–2020 (from 212,300 km^2 to 116,530 km^2).
3. The period of deep convection started later in recent years (Figure 9). For instance, it started about 2 months later in 2018/2019 compared to 2008/2009. The duration of convection has decreased too (Figure 9l). Mixed layers deeper than 250 m were found during about 6 months in 2008 (from November to April) and only during less than 4 months after 2016 (Figure 9l).
4. The Greenland Sea warmed, isopycnals deepened and stratification increased (Figures 6, 7, 10–12). Convection resistance, a measure of the stratification, has doubled over the Greenland Sea (Figure 10e and Figure S5 in Supporting Information S1). These properties changes occurred most strongly in the northeast Greenland Sea (Boreas Basin; Figure 10e and Figures S4 and S5 in Supporting Information S1).
5. At the same time, the Atlantic Water layer expands toward the central Greenland Sea from the Hovgaard Fracture Zone and the Knipovitch Ridge, where the eddy kinetic energy increased from 2015 onward (Figure S6 in Supporting Information S1). This could contribute to the modeled and observed changes in hydrographic properties and wintertime convection. The model also indicates a decrease in the intensity of the Greenland Sea gyre consistent with the isopycnal deepening (Figure 13) while local surface winds and fluxes do not exhibit neither significant trends nor significant interannual variations (Figure S7 in Supporting Information S1).

Argo data clearly support results 1, 2 about deep convection (Figure 5, Figure S3 in Supporting Information S1), 4 on hydrographic changes (Figure 5, Figure S5 in Supporting Information S1). Result 3 is harder to corroborate with Argo data alone (given a lack of continuity in both space and time) however none of the Argo data show an early convection in recent years. Finally, PSY4 gives a dynamical framework which allows to describe the gyre intensity and mesoscale activity (result 5) making the model a valuable complement to observational data.

In this study, we focused on the winter mixed layer depths and winter convection preconditioning. The model is a powerful tool that would also allow to perform volumetric studies to address the production, the residence time within the gyre and the fate of the convected water masses. In particular, the associated exit pathways and contributions to the AMOC lower limb through Denmark Strait and Faroe Bank Channel overflows are a prime research topic (Huang et al., 2020; Q. Wang et al., 2020). Respective contributions to the overflows of new convective areas, developing north of Svalbard (Athanase et al., 2020) and in the boundary currents (Moore et al., 2022; Våge et al., 2018), could also be investigated with the model.

Data Availability Statement

The authors confirm that all the data that support the findings of this study in the main text and Supporting Information S1 are openly available. This study has been conducted using E.U. Copernicus Marine Service Information. The ocean model data used for this study were produced by the global monitoring and forecasting centre operated by Mercator Ocean, and are available for download at https://marine.copernicus.eu. ERA-5 monthly averaged data on single levels are available on the Climate Copernicus Climate Change Service (C3S) Climate Data Store (CDS) website (Copernicus Climate Change Service, 2023). The Argo data were collected and made freely available by the International Argo Program and the national programs that contribute to it (https://argo.ucsd.edu, https://www.ocean-ops.org). The Argo Program is part of the Global Ocean Observing System (Argo, 2000).

Acknowledgments
This work is a contribution to H2020 Arctic Passion project, Grant 101003472. We gratefully thank Camila Artana and Marylou Athanase for their help as well as Jérôme Sirven for early discussions. We deeply thank the two anonymous reviewers whose advice helped us improve the manuscript. Louise Abot acknowledges funding from the H2020 Arctic Passion project, (101003472) and Léa Poli from a Sorbonne Université Ph.D. scholarship.

References

Aksenov, Y., Bacon, S., Coward, A. C., & Holliday, N. P. (2010). Polar outflow from the Arctic Ocean: A high resolution model study. *Journal of Marine Systems*, *83*(1–2), 14–37. https://doi.org/10.1016/j.jmarsys.2010.06.007

Argo (2000). Argo float data and metadata from global data assembly centre [dataset]. SEANOE. https://doi.org/10.17882/42182

Artana, C., Provost, C., Koenig, Z., Athanase, M., & Asgari, A. (2022). Atlantic water inflow through the yermak pass branch: Evolution since 2007. *Journal of Geophysical Research: Oceans*, *127*(2), e2021JC018006. https://doi.org/10.1029/2021JC018006

Årthun, M., Eldevik, T., & Smedsrud, L. H. (2019). The role of Atlantic heat transport in future arctic winter sea ice loss. *Journal of Climate*, *32*(11), 3327–3341. https://doi.org/10.1175/JCLI-D-18-0750.1

Athanase, M., Provost, C., Artana, C., Pérez-Hernandez, M., Sennéchael, N., Bertosio, C., et al. (2021). Changes in circulation patterns in the upper western Nansen basin from 2008 to 2020 according to the Mercator physical system. *Journal of Geophysical Research: Oceans*, *126*(1), e2020JC016825. https://doi.org/10.1029/2020JC016825

Athanase, M., Provost, C., Pérez-Hernández, M., Sennéchael, N., Bertosio, C., Artana, C., et al. (2020). Atlantic water modification north of Svalbard in the Mercator physical system from 2007 to 2020. *Journal of Geophysical Research: Oceans*, *125*(10), e2020JC016463. https://doi.org/10.1029/2020JC016463

Athanase, M., Sennéchael, N., Garric, G., Koenig, Z., Boles, E., & Provost, C. (2019). New hydrographic measurements of the upper arctic western Eurasian basin in 2017 reveal fresher mixed layer and shallower warm layer than 2005–2012 climatology. *Journal of Geophysical Research: Oceans*, *124*(2), 1091–1114. https://doi.org/10.1029/2018JC014701

Bashmachnikov, I., Fedorov, A., Golubkin, P. A., Vesman, A. V., Selyuzhenok, V. V., Gnatiuk, N. V., et al. (2021). Mechanisms of interannual variability of deep convection in the Greenland sea. *Deep Sea Research Part I: Oceanographic Research Papers*, *174*, 103557. https://doi.org/10.1016/j.dsr.2021.103557

Bertosio, C., Provost, C., Athanase, M., Sennéchael, N., Garric, G., Lellouche, J.-M., et al. (2022). Changes in freshwater distribution and pathways in the Arctic Ocean since 2007 in the Mercator ocean global operational system. *Journal of Geophysical Research: Oceans*, *127*(6), e2021JC017701. https://doi.org/10.1029/2021JC017701

Brakstad, A., Våge, K., Håvik, L., & Moore, G. W. (2019). Water mass transformation in the Greenland Sea during the period 1986–2016. *Journal of Physical Oceanography*, *49*(1), 121–140. https://doi.org/10.1175/JPO-D-17-0273.1

Bretones, A., Nisancioglu, K. H., Jensen, M. F., Brakstad, A., & Yang, S. (2022). Transient increase in arctic deep-water formation and ocean circulation under sea ice retreat. *Journal of Climate*, *35*(1), 109–124. https://doi.org/10.1175/JCLI-D-21-0152.1

Chatterjee, S., Raj, R. P., Bertino, L., Skagseth, O., Ravichandran, M., & Johannessen, O. M. (2018). Role of Greenland Sea gyre circulation on Atlantic water temperature variability in the fram strait. *Geophysical Research Letters*, *45*(16), 8399–8406. https://doi.org/10.1029/2018GL079174

Copernicus Climate Change Service, C. D. S. (2023). ERA5 monthly averaged data on single levels from 1940 to present [dataset]. Copernicus Climate Change Service (C3S) Climate Data Store (CDS). https://doi.org/10.24381/cds.f17050d7

Dai, A., Qian, T., Trenberth, K. E., & Milliman, J. D. (2009). Changes in continental freshwater discharge from 1948 to 2004. *Journal of Climate*, *22*(10), 2773–2792. https://doi.org/10.1175/2008JCLI2592.1

Fichefet, T., & Maqueda, M. M. (1997). Sensitivity of a global sea ice model to the treatment of ice thermodynamics and dynamics. *Journal of Geophysical Research*, *102*(C6), 12609–12646. https://doi.org/10.1029/97JC00480

Frajka-Williams, E., Rhines, P. B., & Eriksen, C. C. (2014). Horizontal stratification during deep convection in the Labrador Sea. *Journal of Physical Oceanography*, *44*(1), 220–228. https://doi.org/10.1175/JPO-D-13-069.1

Good, S. A., Martin, M. J., & Rayner, N. A. (2013). EN4: Quality controlled ocean temperature and salinity profiles and monthly objective analyses with uncertainty estimates. *Journal of Geophysical Research: Oceans*, *118*(12), 6704–6716. https://doi.org/10.1002/2013JC009067

Hattermann, T., Isachsen, P. E., von Appen, W.-J., Albretsen, J., & Sundfjord, A. (2016). Eddy-driven recirculation of Atlantic water in fram strait. *Geophysical Research Letters*, *43*(7), 3406–3414. https://doi.org/10.1002/2016GL068323

Hofmann, Z., von Appen, W.-J., & Wekerle, C. (2021). Seasonal and mesoscale variability of the two Atlantic water recirculation pathways in fram strait. *Journal of Geophysical Research: Oceans*, *126*(7), e2020JC017057. https://doi.org/10.1029/2020JC017057

Holliday, N. P., Bersch, M., Berx, B., Chafik, L., Cunningham, S., Florindo-López, C., et al. (2020). Ocean circulation causes the largest freshening event for 120 years in eastern subpolar north Atlantic. *Nature Communications*, *11*(1), 1–15. https://doi.org/10.1038/s41467-020-14474-y

Hu, X., Myers, P. G., & Lu, Y. (2019). Pacific water pathway in the Arctic Ocean and Beaufort gyre in two simulations with different horizontal resolutions. *Journal of Geophysical Research: Oceans*, *124*(8), 6414–6432. https://doi.org/10.1029/2019JC015111

Huang, J., Pickart, R. S., Huang, R. X., Lin, P., Brakstad, A., & Xu, F. (2020). Sources and upstream pathways of the densest overflow water in the Nordic seas. *Nature Communications*, *11*(1), 1–9. https://doi.org/10.1038/s41467-020-19050-y

Johannessen, O. M., & Lygre, K. (1996). Observations of convective chimneys. European subpolar ocean programme. In P. Wadhams, J. P. Wilkinson, & S. C. S. Wells (Eds.), *Sea ice-ocean interactions* (pp. 262–294).

Johannessen, O. M., Sandven, S., & Johannessen, J. A. (1991). Eddy-related winter convection in the Boreas Basin. *Elsevier Oceanography Series*, *57*, 87–105. https://doi.org/10.1016/s0422-9894(08)70062-x

Karpouzoglou, T., de Steur, L., Smedsrud, L. H., & Sumata, H. (2022). Observed changes in the arctic freshwater outflow in fram strait. *Journal of Geophysical Research: Oceans*, *127*(3), e2021JC018122. https://doi.org/10.1029/2021JC018122

Killworth, P. D. (1983). Deep convection in the world ocean. *Reviews of Geophysics*, *21*(1), 1–26. https://doi.org/10.1029/RG021i001p00001
Koenig, Z., Provost, C., Sennechael, N., Garric, G., & Gascard, J.-C. (2017). The Yermak pass branch: A major pathway for the Atlantic water north of Svalbard? *Journal of Geophysical Research: Oceans*, *122*(12), 9332–9349. https://doi.org/10.1002/2017JC013271
Koenig, Z., Provost, C., Villacieros-Robineau, N., Sennechael, N., Meyer, A., Lellouche, J.-M., & Garric, G. (2017). Atlantic waters inflow north of Svalbard: Insights from IAOOS observations and Mercator ocean global operational system during n-ice 2015. *Journal of Geophysical Research: Oceans*, *122*(2), 1254–1273. https://doi.org/10.1002/2016JC012424
Latarius, K., & Quadfasel, D. (2016). Water mass transformation in the deep basins of the nordic seas: Analyses of heat and freshwater budgets. *Deep Sea Research Part I: Oceanographic Research Papers*, *114*, 23–42. https://doi.org/10.1016/j.dsr.2016.04.012
Lauvset, S. K., Brakstad, A., Våge, K., Olsen, A., Jeansson, E., & Mork, K. A. (2018). Continued warming, salinification and oxygenation of the Greenland Sea gyre. *Tellus A: Dynamic Meteorology and Oceanography*, *70*(1), 1–9. https://doi.org/10.1080/16000870.2018.1476434
Lellouche, J.-M., Greiner, E., Le Galloudec, O., Garric, G., Regnier, C., Drevillon, M., et al. (2018). Recent updates to the Copernicus marine service global ocean monitoring and forecasting real-time 1/12 high-resolution system. *Ocean Science*, *14*(5), 1093–1126. https://doi.org/10.5194/os-14-1093-2018
Lien, V. S., Hjøllo, S. S., Skogen, M. D., Svendsen, E., Wehde, H., Bertino, L., et al. (2016). An assessment of the added value from data assimilation on modelled Nordic seas hydrography and ocean transports. *Ocean Modelling*, *99*, 43–59. https://doi.org/10.1016/j.ocemod.2015.12.010
Lique, C., & Thomas, M. D. (2018). Latitudinal shift of the Atlantic meridional overturning circulation source regions under a warming climate. *Nature Climate Change*, *8*(11), 1013–1020. https://doi.org/10.1038/s41558-018-0316-5
Madec, G., & Engine, N. O. (2008). *Note du pôle de modélisation, institut pierre-simon laplace (ipsl)(no. 27)*. France.
Madec, G., & Imbard, M. (1996). A global ocean mesh to overcome the north pole singularity. *Climate Dynamics*, *12*(6), 381–388. https://doi.org/10.1007/BF00211684
Marshall, J., & Schott, F. (1999). Open-ocean convection: Observations, theory, and models. *Reviews of Geophysics*, *37*(1), 1–64. https://doi.org/10.1029/98RG02739
McDougall, T. J., & Barker, P. M. (2011). Getting started with TEOS-10 and the Gibbs seawater (GSW) oceanographic toolbox. *Scor/Iapso WG*, *127*, 1–28.
Moore, G. K., Våge, K., Pickart, R. S., & Renfrew, I. A. (2015). Decreasing intensity of open-ocean convection in the Greenland and Iceland seas. *Nature Climate Change*, *5*(9), 877–882. https://doi.org/10.1038/NCLIMATE2688
Moore, G. K., Våge, K., Renfrew, I. A., & Pickart, R. S. (2022). Sea-ice retreat suggests re-organization of water mass transformation in the Nordic and Barents seas. *Nature Communications*, *13*(1), 1–8. https://doi.org/10.1038/s41467-021-27641-6
Mork, K. A., Skagseth, Ø., & Søiland, H. (2019). Recent warming and freshening of the Norwegian sea observed by Argo data. *Journal of Climate*, *32*(12), 3695–3705. https://doi.org/10.1175/JCLI-D-18-0591.1
Orvik, K. A., & Niiler, P. (2002). Major pathways of Atlantic water in the northern north Atlantic and Nordic seas toward arctic. *Geophysical Research Letters*, *29*(19), 2–1. https://doi.org/10.1029/2002GL015002
Piechura, J., & Walczowski, W. (1995). The arctic front: Structure and dynamics. *Oceanologia*, *37*(1), 47–73.
Polyakov, I. V., Pnyushkov, A. V., Alkire, M. B., Ashik, I. M., Baumann, T. M., Carmack, E. C., et al. (2017). Greater role for Atlantic inflows on sea-ice loss in the Eurasian basin of the Arctic Ocean. *Science*, *356*(6335), 285–291. https://doi.org/10.1126/science.aai8204
Quadfasel, D., & Meincke, J. (1987). Note on the thermal structure of the Greenland Sea gyres. Deep sea research Part A. *Oceanographic Research Papers*, *34*(11), 1883–1888. https://doi.org/10.1016/0198-0149(87)90061-6
Schauer, U., Beszczynska-Möller, A., Walczowski, W., Fahrbach, E., Piechura, J., & Hansen, E. (2008). Variation of measured heat flow through the fram strait between 1997 and 2006. In *Arctic–subarctic ocean fluxes* (pp. 65–85). Springer. https://doi.org/10.1007/978-1-4020-6774-7_4
Schlosser, P., Bönisch, G., Rhein, M., & Bayer, R. (1991). Reduction of deepwater formation in the Greenland Sea during the 1980s: Evidence from tracer data. *Science*, *251*(4997), 1054–1056. https://doi.org/10.1126/science.251.4997.1054
Våge, K., Papritz, L., Håvik, L., Spall, M. A., & Moore, G. W. (2018). Ocean convection linked to the recent ice edge retreat along east Greenland. *Nature Communications*, *9*(1), 1–8. https://doi.org/10.1038/s41467-018-03468-6
von Appen, W.-J., Schauer, U., Hattermann, T., & Beszczynska-Möller, A. (2016). Seasonal cycle of mesoscale instability of the west Spitsbergen current. *Journal of Physical Oceanography*, *46*(4), 1231–1254. https://doi.org/10.1175/JPO-D-15-0184.1
Walczowski, W. (2013). Frontal structures in the west Spitsbergen current margins. *Ocean Science*, *9*(6), 957–975. https://doi.org/10.5194/os-9-957-2013
Wang, Q., Wekerle, C., Wang, X., Danilov, S., Koldunov, N., Sein, D., et al. (2020). Intensification of the Atlantic water supply to the Arctic Ocean through fram strait induced by arctic sea ice decline. *Geophysical Research Letters*, *47*(3), e2019GL086682. https://doi.org/10.1029/2019GL086682
Wang, X., Zhao, J., Hattermann, T., Lin, L., & Chen, P. (2021). Transports and accumulations of Greenland Sea intermediate waters in the Norwegian Sea. *Journal of Geophysical Research: Oceans*, *126*(4), e2020JC016582. https://doi.org/10.1029/2020JC016582